Bulletin of Earthquake Engineering
https://doi.org/10.1007/s10518-026-02450-8

ORIGINAL ARTICLE

Numerical simulation of shaking table tests on two modern URM buildings using equivalent-frame modeling

Stefania Degli Abbati[1] · **Hervé Degée**[2] · **Sergio Lagomarsino**[1] · **Serena Cattari**[1]

Received: 30 October 2025 / Accepted: 22 March 2026
© The Author(s) 2026

Abstract
This paper presents the results of the numerical analyses conducted to reproduce the shake table tests performed in Lisboa at the LNEC laboratory (Laboratório Nacional de Engenharia Civil) on two full-scale masonry prototypes. The equivalent frame modeling strategy was chosen as an effective compromise between computational efficiency and accuracy in simulating the seismic behavior. The model was developed using a blind prediction approach, like that typically employed by practitioners in seismic assessments of existing buildings. Based on geometry and construction details, appropriate modeling strategies were implemented to capture the nonlinear behavior of structural elements. A piecewise-linear constitutive law was applied and, as a novel contribution, the flange effect was incorporated using an equivalent beam, calibrated with a practice-oriented analytical expression that accounts for geometry and material characteristics of the web and flange. Experimental data from panels with similar masonry were used to calibrate the strength parameters at the structural element scale. Another relevant contribution was the validation of EF models in predicting the seismic response of modern masonry typologies with box-like behavior under increasing levels of nonlinearity and structural irregularity in the two prototypes. To this aim, nonlinear dynamic simulations replicating the shaking table tests were performed and compared with the experimental results. Traditional techniques were combined with more innovative tools to manage the large volume of experimental data and gain insights into the prototypes' response. The numerical analyses successfully reproduced the experimental behavior across the full set of data and for both models, without the need for further refinement.

Keywords Masonry · Nonlinear dynamic analyses · Model calibration · Equivalent frame model

Extended author information available on the last page of the article

Published online: 21 April 2026

1 Introduction

The use of numerical models for predicting the seismic response of existing structures is a relevant topic, given its potential repercussions also on engineering practice. Two key challenges arise in the application of numerical models: first, the need to address appropriate modeling choices based on often limited data regarding mechanical parameters and construction details; and second, the reliability of these models in predicting the actual structural response. Several studies have been conducted in recent years to explore these topics. These studies can be classified into benchmarking studies, which test various modeling strategies on shared benchmark case studies (Salonikos et al. 2003, Marques and Lourenço 2011; Giamundo et al. 2014; Betti et al. 2015; Bartoli et al. 2017; Aşıkoğlu et al. 2020; Malcata et al. 2020), and blind predictions, which aim to predict the seismic response of experimental prototypes before testing (Mendes et al. 2017; Esposito et al. 2019; Calderini et al. 2024; Tomic et al. 2024). Although these studies differ in the number of examples considered, constructive features, software used, and modeling assumptions, they all emphasize the significant scatter in the obtained results. This variation stems from many sources of uncertainties affecting the seismic assessment of buildings, such as: different methods for selecting material properties; assumptions made in defining the numerical model, which involve many possible approaches to simulate the seismic behavior of existing structures (Lourenco 2002; Roca et al. 2010; D'Altri et al. 2020); alternative options to select analysis types; structural and morphological complexity, which may lead to different assumptions in the modeling process (Cattari et al. 2022; Rota et al. 2014; Bracchi et al. 2015); the lack of standardized procedure to define limit states and finalize the verification; for assessments based on nonlinear procedures, solution that may not be unique and that are dependent on the convergence algorithm used (Cattari et al. 2022); and the challenges associated with interpreting the results.

Recent blind prediction studies (e.g., Tomic et al. 2024 and Calderini et al. 2024) have clearly shown that numerical results can differ significantly from experimental outcomes, primarily due to challenges in selecting modeling strategies that consistently capture the actual structural response. Although the variability in results tends to decrease when input data are shared, a certain degree of dispersion persists, as shown in the ReLUIS benchmark project by Cattari and Magenes 2022. This remains true even when detailed surveys on geometry, construction details, and material test data are available (as highlighted by Malcata et al. 2020), partly due to difficulties in correlating data from the material scale to the panel scale. Benchmarking and blind prediction exercises have consistently shown that while qualitative aspects—such as collapse mechanisms and crack patterns—are often reasonably well captured, substantial scatter remains in the prediction of quantitative parameters, including capacity curves, accelerations, and displacements (Parisse et al. 2021; Calderini et al. 2024). Furthermore, structural complexity plays a critical role: the more complex the case study, the greater the sensitivity of the predicted response to modeling choices and the resulting variability. This trend is particularly evident in the blind predictions of aggregate structures presented by Tomic et al. 2024; where high dispersion was observed despite limited uncertainty in material and structural characteristics.

Anyway, the comparison between the results of blind predictions and postdictions highlights that the numerical models, when calibrated using dynamic identification tests and refined exploiting experimental data and outcomes, can properly describe the structural

seismic response or, at the very least, improve their predictive capabilities (Aşıkoğlu et al. 2024; Bianchini et al. 2024; Malomo and DeJong 2022; Tomic and Beyer 2024). However, it is worth noting that dynamic identification data or in-situ tests on materials and components are often unavailable in engineering practice due to high costs or practical limitations. Consequently, developing a numerical model that can reasonably predict the actual seismic response, relying solely on a few parameters easily obtainable from the knowledge phase, is equally relevant and challenging.

In this context, this paper addresses the issue of numerical model validation based on experimental data through a blind prediction approach. Unlike many previous studies, where postdictions address model calibration and parameters and modeling assumptions are adjusted after comparing numerical results with experimental outcomes, this study exploits solely information typically available in engineering practice, replicating the procedure applied by practitioners in the seismic assessments of existing buildings. The experimental results are used in this study to assess the validity of the initial modeling assumptions.

Data from shaking table tests on two full-scale prototypes conducted at the Laboratório Nacional de Engenharia Civil (LNEC) were used as a benchmark for validation (§ 2). The available information on geometry and constructive details was used to set up an equivalent frame (EF) model operating at the scale of the structural element aimed at reproducing the expected seismic behavior (§ 3.1). The parameters required to define the nonlinear response of masonry panels were calibrated using results from another experimental campaign on panels with masonry typologies similar to those of the tested prototypes (§ 3.2), as only a limited number of tests on constituent materials were conducted on the two full-scale structures. Data from dynamic vibration tests were then used to assess the variation between the numerical and experimental frequencies. Finally, nonlinear dynamic analyses (NLDA) were performed to simulate the shaking table tests, comparing the numerical results with the experimental data (§ 4).

While several studies have demonstrated the reliability of the EF modeling approach in predicting the seismic response of complex existing unreinforced masonry (URM) buildings governed by global in-plane mechanisms (e.g., Ottonelli et al. 2022; Degli Abbati et al. 2022; Requena-Garcia-Cruz et al. 2023), its validation for modern masonry typologies with box-like behavior remains limited. Addressing this gap represents the first original contribution of this study. As a second novel contribution, the flange effect was incorporated into the EF models through an equivalent beam, calibrated using a practice-oriented analytical expression that accounts for the geometry and material characteristics of the *web* and *flange*. Furthermore, the complex sequence of ground motions that characterizes this experimental campaign, comprising multiple shakes of increasing intensity and applied in alternating directions (§ 2.1), constituted an opportunity to evaluate the EF model's capability in capturing the progression of nonlinear behavior and reproducing the seismic response of two structures with different levels of irregularity. This represents a further novelty of this study. Finally, two analytical tools were applied to the experimental and numerical outcomes to manage the large amount of experimental data, characterize the expected seismic behavior, and interpret the dynamic response observed during the tests, as detailed in § 2.3. The first tool uses a Fourier transform to analyze the acceleration time histories recorded on the shake table and those filtered by the experimental prototypes. It was used to identify the fundamental periods in the elastic phase and track their elongation as damage increased. These fundamental periods were then compared with those obtained using a second tool, which is

based on a MATLAB algorithm. This algorithm approximates the displacement time histories recorded on the prototypes by simulating the response of an equivalent linear oscillator subjected to the same accelerations. It varies the number of degrees of freedom and selects the configuration that minimizes the error.

2 Experimental shake-table test campaign

This Section provides an overview of the key features of the test units, setup, and experimental results from the full-scale shaking table tests conducted at the Laboratório Nacional de Engenharia Civil (LNEC). For more detailed information, readers are referred to Jäger et al. 2015.

2.1 Experimental models, test programs, and instrumentations

The test units consisted of two full-scale 2-story buildings (labeled as *Model A* and *Model B*), each with ground floor dimensions of 3.7×4.2 m² and a total height of 5.4 m. The walls were 20 cm thick. These units were constructed on steel foundations specifically designed for this purpose by the University of Liège. The units were built using premium insulation-filled clay blocks from Wienerberger, with a thin mortar layer approximately 1 mm thick. These modern blocks, characterized by relatively large voids to place additional insulation material, were designed to provide good mechanical properties and excellent thermal insulation, ensuring compliance with stringent energy efficiency regulations for heating and cooling demand. The intermediate floor and the roof were made of 20 cm-thick reinforced concrete (R.C.) slabs. To simulate an equivalent accidental load equal to 2 kN/m^2, four masses of 6 kN each were placed on the intermediate floor. The masses were symmetrically positioned around the center of gravity of the slab to replicate the inertial effects of a uniformly distributed load. Figure 1 shows the floor plans of both models and a general view of *Model B*. *Model A* is regular and symmetric, while *Model B* has a strongly irregular layout of the openings in the façade.

The mechanical and geometrical parameters of blocks, mortar joints, and masonry are collected in Table 1.

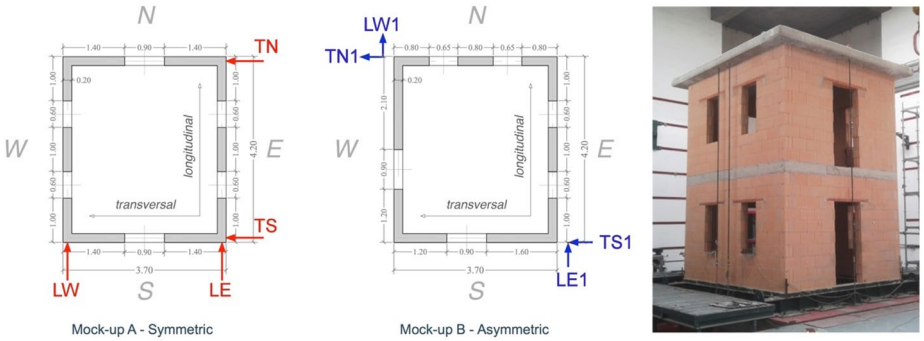

Fig. 1 Geometrical plans of **a**) *Model A* and **b**) *Model B*; **c**) View of *Model B* in the LNEC laboratory before the tests (from Cattari et al. 2014)

Table 1 Mechanical parameters of masonry (a) and constituents (b-blocks; c-mortar)

a- Masonry	
Mean compressive strength f_i (EN 1052-1) [N/mm²]	5.6
Characteristic compressive strength f_k (EN 1052-1) [N/mm²]	5.3
Young Modulus (EN 1052-1) [N/mm²]	4500
Characteristic shear strength f_{vk0} (EN 1052-1) [N/mm²]	0.32
b-Blocks	
Mean compressive strength $\bar{f}_b$ (EN 772-1) [N/mm²]	10.7
Normalized compressive strength f_b (EN 772-1) [N/mm²]	13.4
Void percentage (EN 772-3) [%]	48
Density (EN 772-3) [kg/m³]	755
Dimensions L x H x W (EN 772 − 16) [mm]	400 × 249 × 200
c-Mortar	
Flexural strength (EN 1015-11) [N/mm²]	3.1
Compressive strength (EN 1015-11) [N/mm²]	12.1
Density (EN 1015-6) [g/cm³]	1.39

Fig. 2 Constructive steps of the test units (pictures adapted from Mendes et al. 2014 and https://pdfs.semanticscholar.org/040a/276c21300b617fb4b6f38a583b0c0fba0ac5.pdf)

The test units were built simultaneously in the laboratory. After 28 days of masonry curing, they were placed on the shake table for testing. Figure 2 shows pictures of the construction process, from the steel foundation (Fig. 2a) to the final models (Fig. 2b-c-d).

The input used for the shake table tests was a semi-artificial earthquake. It was derived from the two components of the 1976 Friuli earthquake recorded at the Tolmezzo Station,

Table 2 Test program, number of runs, and load sequence applied to the test units

Model A (symmetric)				*Model B* (asymmetric)			
Run	**NS (Long.)**	**EW (Trans.)**	**No. of shakes**	**Run**	**NS (Long.)**	**EW (Trans.)**	**No. of shakes**
01T	-	0.04g	6	01T	-	0.04g	5
01L	0.045g	-	5	01L	0.045g	-	5
02	0.09g	0.08g	5	02	0.09g	0.08g	6
03T	-	0.12g	5	03T	-	0.12g	5
03L	0.135	-	5	03L	0.135	-	4
04	0.18	0.16	5	04	0.18	0.16	5
05T	-	0.20g	5	05T	-	0.20g	4
05L	0.225g	-	6	05L	0.225g	-	5
06	0.27g	0.24g	6	06	0.27g	0.24g	6
07T	-	0.28	7	07L	0.315	-	4
07L	0.315	-	5	07T	-	0.28	3
08	0.36	0.32	2	08	0.36	0.32	2
Total No. of shakes			62	Total No. of shakes			54

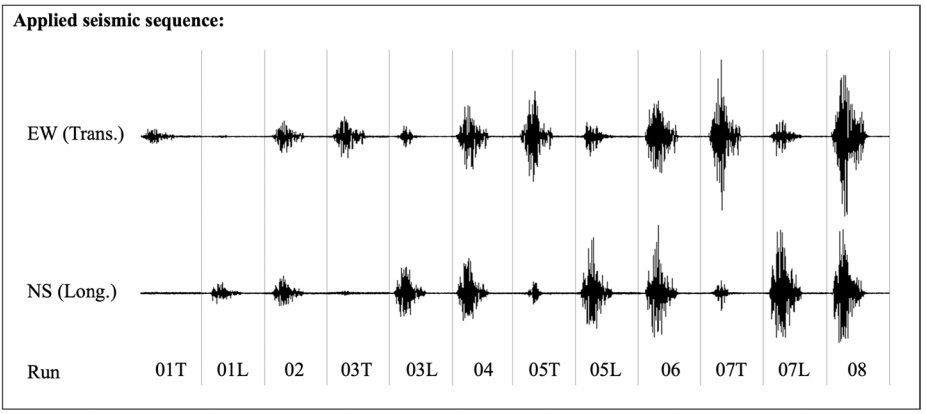

which were properly modified to match a specific EC8 elastic response spectrum (see Lu et al. 2014 for details). The N-S component, applied in the longitudinal direction during the tests, was scaled to a PGA = 0.36 g, while the E-W component, applied in the transversal direction during the tests, was scaled to a PGA = 0.32 g. The shake table testing program consisted of eight runs identified by a number in Table 2.

The downscaling applied to the input in each run was: 12.5%, 25%, 37.5%, 50%, 62.5%, 75%, and 87.5%. After each run, dynamic identification tests were performed to track changes in the fundamental periods and to monitor damage evolution. As the shake-table's movement does not perfectly replicate the input record due to control system feedback, an adaptive technique was applied to minimize the differences between actual and target motions. The input motions were progressively increased at each step to achieve the final target intensity (see Lu et al. 2014 for more details). As a result, *Model A* underwent 62 total shakes, while *Model B* underwent 54 (Table 2). Table 2 summarizes the PGAs applied in the load sequence for the eight runs.

The instrumentation system installed on the mock-ups includes unidirectional piezoelectric accelerometers, LVDTs, and an optical system composed of LED displacement transducers. A detailed layout of the sensors on the façades of the mock-ups is provided in Lu et

al. (2014), while Fig. 1 shows the plan view indicating the locations of the accelerometers (red arrows) and LED transducers (blue arrows) installed at the level of the two RC slabs (intermediate floor and rooftop) on both mock-ups, following identical configurations. The acronyms used in Fig. 1 are defined as follows: T and L indicate Transverse and Longitudinal accelerations (or displacements), while N, S, E, and W refer to the North, South, East, and West façades.

2.2 Test observations and experimental results

The test units underwent eight cycles, with PGAs ranging from 0.04 to 0.36 g, resulting in a performance ranging from minor damage to near collapse. After each seismic run, dynamic identification tests were performed to detect the main modes, their corresponding natural frequencies, and their evolution during the tests. Figure 3 shows the frequency evolution for the two models obtained from dynamic identification tests after runs 1, 2, 4, 6, and 8. The results indicate that the fundamental frequencies are equal to 5.7 and 6.9 Hz for *Model A* (longitudinal and transversal directions, respectively) and 5.4 and 5.8 Hz for *Model B*. Furthermore, the results show that in both models, the frequencies decrease as the acceleration levels of the input record increase. Although this trend is observed in both directions, it is more pronounced in the transverse (W-E) direction for both models, which aligns with the damage pattern at the end of the tests, showing greater degradation and collapse mechanisms along this direction.

The damage progression and failure modes observed in the two test units are summarized below, along with the key results. A detailed description of the experimental seismic response can be found in Jäger et al. 2015 and Lu et al. 2014. Instead, Sect. 4 will compare the experimental data and numerical predictions based on the equivalent frame modeling approach.

In *Model A*, the damage was primarily concentrated on the second level, particularly on the north and south facades, indicating that the transverse direction was the most vulnerable. The crack patterns on these walls suggest the activation of a shear mechanism, driven by

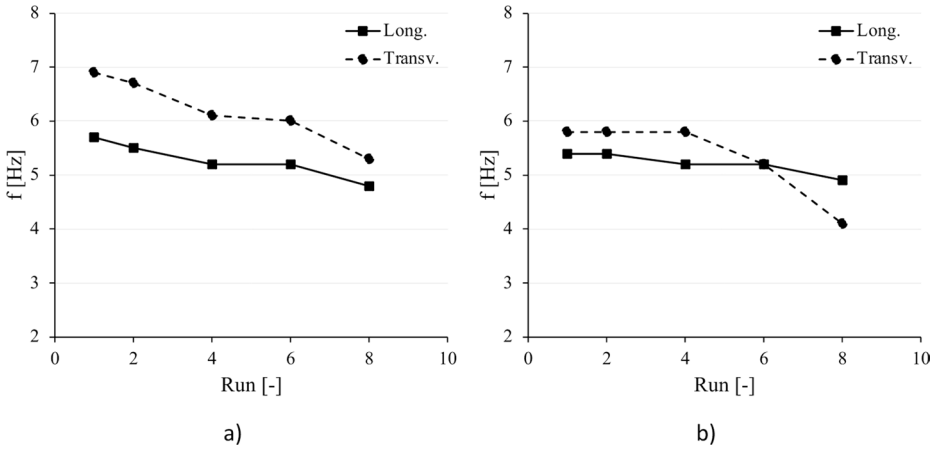

Fig. 3 Frequency evolution from dynamic identification tests (runs 1, 2, 4, 6, and 8): **a**) *Model A;* **b**) *Model B*

tangential stresses generated by horizontal forces combined with normal stress components. Diagonal cracks were mostly concentrated in the joints. The sliding of blocks along the horizontal mortar joints led to further separation of the dry vertical joints. A prominent vertical crack in the upper part of the west wall indicates lateral sliding of the masonry pier in the north wall, which defines the northwest corner of the second floor.

Conversely, in *Model B*, the damage was more concentrated on the first level, where normal compressive stresses were higher. As in *Model A*, shear mechanisms were the predominant failure mode. The damage was particularly severe on the masonry pier on the ground floor between the two windows on the north wall, where the block sliding nearly caused the collapse of the entire structure. The 'stair-step' cracks on both the north and south walls indicate shear failure. Furthermore, a horizontal sliding crack is visible on the south wall at the second mortar joint, starting from the foundation level. Figure 10 shows the crack patterns of the two models at the end of the shake table test.

2.3 Tools used for the interpretation of the results

The availability of data from shake-table tests on full-scale mock-ups is a valuable tool for validating numerical models. However, processing large amounts of experimental data requires techniques to characterize the expected seismic behavior and interpret the dynamic response observed during the tests. To this end, both traditional and more innovative tools were applied in this paper. Firstly, the experimental accelerations and displacements were processed to obtain the hysteretic curves, which were then compared with those derived numerically through NLDA. The comparison of hysteretic curves, along with the simulated and predicted damage patterns, allows the Authors to assess whether the numerical model can represent the expected global behavior and relevant failure modes of the two test units. Next, two tools were employed to characterize the dynamic behavior of the experimental models. The first tool analyzes acceleration signals recorded at the shake table and on the mock-ups by applying a Fourier transform, converting the data from the time domain to the frequency domain. In this domain, transfer functions are calculated as the ratio of the Fourier transform of the output signal (measured on the test units) to that of the input signal (measured at the shake table). These functions describe how the system responds at different frequencies and enable the identification of natural frequencies, which appear as peaks in the magnitude of the transfer function. By tracking the shifts in these peaks over time, the tool allows for the monitoring of structural degradation as damage progresses. The second tool identifies the fundamental frequencies by defining an equivalent linear oscillator. A MATLAB algorithm (Van Overschee and De Moor 1994) was used to approximate the experimental displacement time histories measured on the mock-up using the response of this equivalent linear system subjected to the same accelerations. The algorithm varies the number of degrees of freedom and selects as a target the system with the lowest error in simulating the experimental response.

Table 3 summarises the two techniques used to interpret the experimental results, clarifying the necessary input data and the output obtained. It must be specified that the two above-mentioned techniques have been applied first to the experimental results, and then they were used to process the results of the NLDA performed on the numerical model set up to reproduce the experimental behavior (§ 4.2).

Table 3 Summary of the techniques used to interpret the experimental results, and input and output data

Technique	Input data	Output data
Frequency analysis	Acceleration time histories on the shaking table and transmitted to the test unit	Natural frequencies of vibrations
Equivalent oscillator	Acceleration time histories on the shaking table and displacement time histories transmitted to the test unit	Natural frequencies and damping factors

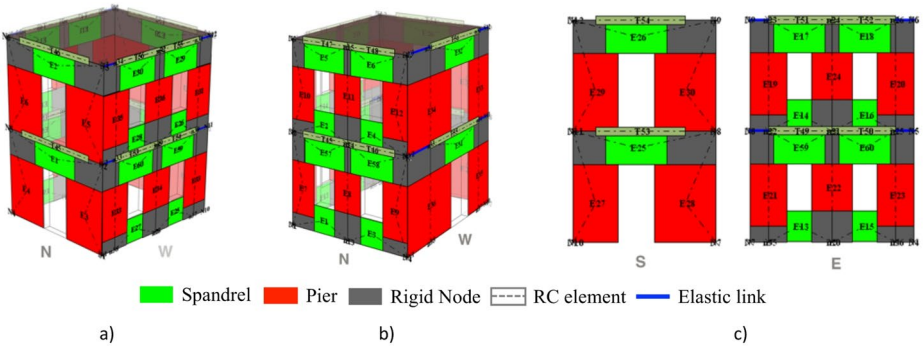

Fig. 4 EF model of the two test units: **a**) *Model A* and **b**) *Model B*; **c**) Mesh of two façades of *Model B*

3 Selected modeling strategies and mechanical parameters of the numerical models

This section provides an overview of the key assumptions made in the modeling process and the definition of the mechanical properties used to set up the numerical model. It is important to note that, in this study, the numerical models of the two test units were developed using an approach similar to a blind prediction. Specifically, the models were created using available data on materials and construction details, employing reliable modeling strategies to predict the expected response, without any calibration or refinement after comparing them with the experimental data. This workflow was applied to replicate the methodology typically used by practitioners in the seismic assessment of existing buildings.

3.1 EF modeling assumptions

The modeling strategy assumed to reproduce the experimental behavior exhibited by the two test units was the EF model approach adopted by the Tremuri software package (Lagomarsino et al. 2013). According to this approach, each URM wall is divided into piers and spandrels that are deformable and connected by rigid nodes. The nonlinear response is concentrated in piers and spandrels, as cracks are typically observed in these areas during earthquakes. Diaphragms are modelled in Tremuri as finite orthotropic membrane elements with a Young's modulus E_{1D} along the floor span, which is considered the principal direction, a Young's modulus E_{2D} along the perpendicular direction, the Poisson's ratio v, and the shear modulus G_D. The three-dimensional structure is then built up as an assemblage of floors and walls, which contribute to the overall response with their in-plane strength and stiffness. Figure 4 shows a 3D view of the two EF models and the mesh of the main façades.

The deformable elements are modelled as nonlinear beams with lumped inelasticity idealization by adopting the piecewise-linear constitutive law implemented in Tremuri and described in Cattari and Lagomarsino 2013 (Fig. 5a). This constitutive law is based on a phenomenological approach. It allows the user to define the initial stiffness of the panel and its progressive degradation, the maximum strength (V_y), the progress of the nonlinear response until severe damage levels (from 1 to 5), and the hysteretic response. The beam theory defines the elastic phase through the definition of the elastic Young modulus E and shear modulus G, while a secant stiffness approximates the progressive degradation. The secant stiffness is defined by assigning a proper ratio between the initial stiffness (k_{el}) and the secant stiffness (k_{sec}) – see Fig. 5a. The nonlinear response is described through progressing strength decay (β_{Ei}) in correspondence with assigned drift values (θ_{Ei}). Different values of θ_{Ei} and β_{Ei} are assigned for the prevailing flexural or shear response of the panel and may be differentiated for spandrels or piers. For the hybrid failure mode, the software package computes average values for θ_{Ei} and β_{Ei} starting from those assigned by the user for flexural or shear failure modes. The user can also govern the occurrence of a mixed failure mode by defining an admissible range in the V-N domain around the intersection point between flexural and shear domains, as shown in Fig. 5b.

The simplified criteria proposed in the literature to describe possible panel failure modes (i.e., crushing, bed joint sliding, shear diagonal cracking, as discussed in Calderini et al. 2009) are applied to compute the maximum strength, which is evaluated as the minimum value among the predictions from the strength domains. In this study, the *flexural* response was calculated according to the beam theory, assuming no tensile strength for masonry. Instead, the *shear* response was described by the Mann and Muller 1982 criterion. Table 4 summarizes the formulas implemented in Tremuri to describe the strength criteria of URM panels used in this paper. The R.C. ring beams placed in the test units at the floor level and the rooftop were also modeled as 2D nonlinear beams with plastic hinges in the end sections (Cattari and Lagomarsino 2013).

The reliability of the EF approach in describing the response of URM buildings has been extensively demonstrated in past studies, such as Marino et al. 2019; Brunelli et al. 2020; Ferrero et al. 2024.

Finally, the so-called *flange effect* was taken into consideration. It is worth noting that *flanges*, which are the piers loaded out of their plane, may affect the failure modes, maximum strength, and displacement capacity of the *web*, which is the in-plane loaded pier

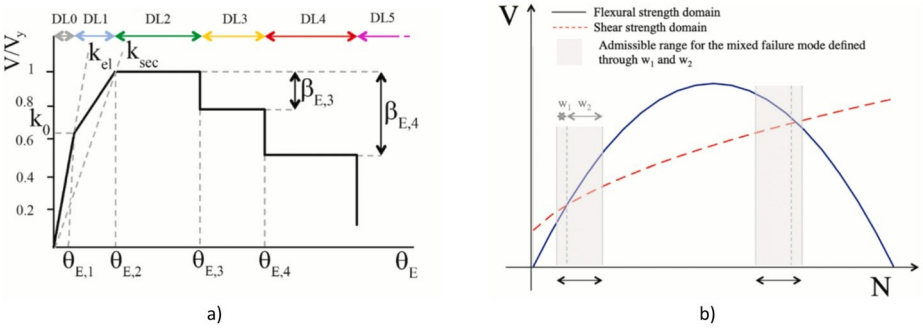

Fig. 5 **a**) Piecewise-linear constitutive law; **b**) Sketch of the criteria assumed to define a hybrid failure (figure adapted from Cattari et al. 2021)

Table 4 Strength criteria that are used to interpret the flexural and shear response of URM panels

Expression		Reference
$V_{u,pf} = \frac{lt\,p}{2\alpha_v}\left(1 - \frac{p}{\kappa f_m}\right)$	(1)	EN 1998-3 2005, NTC 2018
$V_{M\&M,shear} = \frac{lt}{b}(\bar{c} + \bar{\mu}p) \leq \frac{lt}{b}\frac{f_{bt}}{\beta_1}\sqrt{1 + \frac{p}{f_{bt}}}$	(2)	Mann and Muller 1982

Involved parameters:
$\alpha_v = \psi\ (h/l)$: coefficient governing the panel's boundary conditions; k = 0.85; l, t and h: transversal length, thickness, and panel's height; b: coefficient accounting for the mean shear stress at the center of the panel (values ranging from 1 to 1.5, based on the panel's slenderness); $\bar{c}$ and $\bar{\mu}$: equivalent cohesion and friction coefficient, based on the local friction coefficient μ, the cohesion c of mortar joints, the length Δ_x and the height Δ_y of the unit; p: mean compressive stress on the panel; f_{bt}: tensile strength of the unit; β_1: coefficient computed as a function of the shape of the unit (here assumed equal to 1.67).

(Cattari et al. 2023). Although codes suggest rules to compute the *flange* effective width in a single panel subjected to in-plane response, all intersecting panels must be considered in a 3D model of the building to account for torsional behavior and to characterize the response in both orthogonal directions. However, if all intersecting piers are considered perfectly coupled, the *flange effect* is overestimated. Thus, to simulate the actual length of the orthogonal pier where stress distribution is possible, an equivalent beam has been introduced between the nodes at the top of the piers. The practice-oriented formula proposed by Cattari et al. 2023 (Eq. 1) was applied to compute the transversal area A_B of the equivalent beam and calibrate the equivalent shear stiffness based on the geometry and mechanical properties of the *web* and the *flange*:

$$A_B = l_B\omega\frac{12(1+v_W)A_W}{5h\left(\frac{1+\zeta}{\zeta} + \frac{12d^2}{l_W^2\left(1+\frac{E_F J_F}{E_W J_W}\right)}\right)} \cong l_B\omega\frac{12(1+v_W)A_W}{5h\left(\frac{1+\zeta}{\zeta} + \frac{12d^2}{l_W^2}\right)} \quad (1)$$

The parameters involved in A_B are: the beam length l_B, the interstory height h, the *web* area A_W, the moment of inertia of the *web* and of the *flange* (J_W and J_F), the *web*'s width l_W, the Young's moduli of masonry (E_W and E_F), the Poisson coefficient of the *web* v_W (assumed for the equivalent beam's material as well), the distance d between the *web* centroid and the *flange* middle plane, a dimensionless factor $\zeta = \frac{E_F A_F}{E_W A_W}$, and the parameter ω that governs the degree of connection and that has been assumed equal to ω =2 in this study.

3.2 Calibration of the mechanical parameters

The calibration of mechanical parameters is a crucial step in seismic assessment, as it significantly influences the reliability of numerical predictions. However, it is also a challenging task, particularly due to the difficulty of consistently linking material-scale properties to the target panel-scale mechanical properties defined in standards, which are often used as input data in some modeling strategies, such as the EF approach adopted in this paper (Cattari et al. 2022; D'Altri et al. 2021; Parisse et al. 2022). In the examined case, only a few tests were performed on individual constituents and assemblages of masonry (Table 1 in § 2.1, Degée

et al. 2007), obtaining the mechanical properties at the material scale (blocks and mortar). Since the EF model works directly at the element scale (i.e., the piers and spandrels), tests on panels are useful for evaluating the parameters involved in the strength criteria used as a reference here (§ 3.1). Therefore, the parameters necessary to describe the nonlinear response of URM panels were calibrated starting from the results of an experimental campaign performed on similar masonry typologies. The latter has been conducted at the University of Kassel, as part of the ESECMaSE project (Enhanced Safety and Efficient Construction of Masonry Structures in Europe, www.esecmase.org). Among the various masonry types tested in this extensive campaign, the results from panels made of optimized bricks (types 1 or 2) using thin-layer mortar (test n° 5, 7, 9, 10, 12, 13, 14, 15) have been adopted (Fig. 6). These panels were selected as they have a hole pattern like the Wienerberger blocks used in the shaking table campaign. Table 5 presents the main features of the ESECMaSE panels chosen for the parameter calibration. The table includes the type of brick (unit type), panel id (*N.*°), thickness (t), length (l), height (h), slenderness (λ), mean compressive strength of masonry (f_m), coefficient accounting for the panel boundary conditions (ψ), observed failure mechanism (distinguishing between a shear S or flexural F prevailing mechanisms), and crack pattern (as specified in the legend of the table).

Figure 7 shows the comparison between the experimental results of some panels (red indicators) and the predictions of the strength criteria adopted in the EF models. Obviously, the panels have been selected to calibrate the mechanical parameters on which the corresponding strength criteria are based, depending on the prevailing failure mechanisms.

The failure domains are expressed in terms of maximum strength V and ratio p/f_m, where p is the normal vertical stress normalized by the masonry mean compressive strength f_m. The shear failure domain (black curve in Fig. 7) was determined according to Eq. (2) in Table 4 as the minimum value between the activation of two different mechanisms: shear failure of

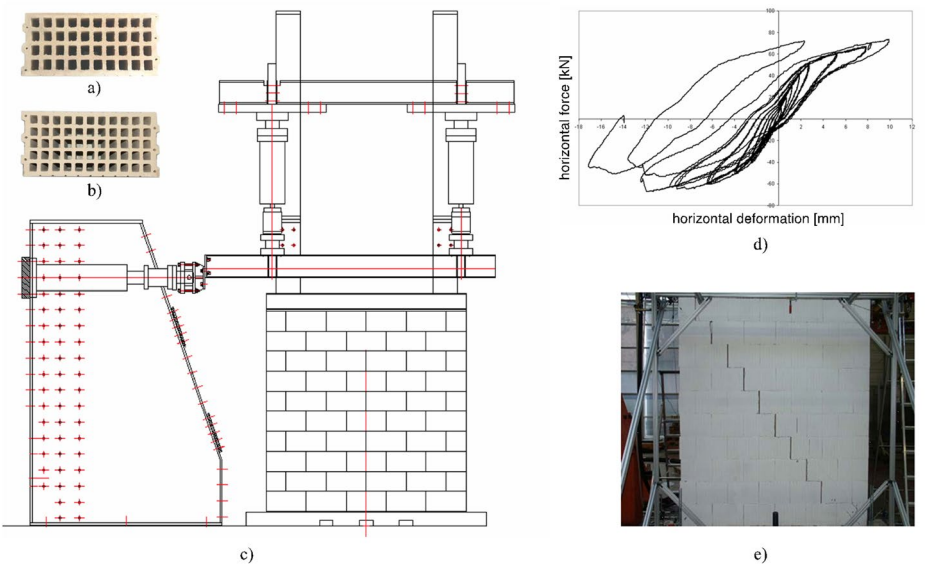

Fig. 6 The ESECMaSE panels used for the calibration of the mechanical parameters: **a**) optimized clay unit type 1; **b**) optimized clay unit type 2; **c**) Test set-up; **d**) Experimental hysteresis curve; **e**) Observed crack pattern in wall N.° 9 (figure from Cattari et al. 2014)

Table 5 Features of the ESECMaSE panels selected for the calibration of parameters

Unit type	*N.*°	t [m]	l [m]	h [m]	λ =h/l [-]	f_m [MPa]	ψ [-]	Failure mechanism	Crack pattern
Opti.1	5		2.2		1.14			S	Db
	7		1.1		2.27			S	Dmj
	9		2.2		1.14			S	Dmj
Opti.2	10	0.175	2.2	2.5	1.14	6.7	0.5	S	Db
	12		1.1		2.27			F	C
	13		1.1		2.27			S	Db
	14		1.1		2.27			F	R
	15		2.2		1.14			S	Dmj

Legend: Failure mechanism: S – shear; F: flexural. Crack pattern: Dmj-Diagonal crack in mortar joints; Db-Diagonal crack in blocks; C-crushing; R-rocking

the panel with typical "stair-step" cracks (experimentally observed in panel 10) and shear failure with cracks on the blocks (experimentally observed in panel 15). The corresponding failure domains are represented by dashed lines and labeled in Fig. 7 as *"Shear-joint"* and *"Shear-block"*, respectively. The flexural domain, described by Eq. (1) in Table 4, is represented by the grey curve in Fig. 7. Figure 7 shows that the parameters derived from the experimental campaign on ESECMaSE panels provide a good reproduction of the failure domain of the panels.

Tables 6 and 7 summarize the parameters used in the numerical simulations in the linear and nonlinear fields. It must be specified that, starting from the experimental results of the ESECMaSE panels, some modifications have been applied based on expert judgment to account for the peculiarities of the masonry adopted in the shake table experimental campaign. The same mechanical parameters were adopted for both models. As for the drift limits reported in Table 7, the assumed parameters are consistent with the results of in-plane cyclic tests on modern brick masonry piers found in the literature (Morandi et al. 2018).

After setting up the numerical model, a modal analysis was performed in Tremuri to identify the dynamic properties of the main modes (i.e., frequencies and participant masses in the orthogonal directions). The values assumed for the Young and shear moduli in the elastic condition were derived by reducing the stiffness parameters available from the experimental campaign on masonry wallets (Table 1) to achieve the best fit between numerical and experimental data. This reduction is also consistent with what was observed and applied in other studies, e.g., in the post-diction numerical simulations of a shake-table test on an aggregate building presented by Bianchini et al. 2024. Moreover, the reduction employed in this study accounts for and balances several factors: the inherently higher stiffness of the EF model, due to the inclusion of rigid areas, and the initial cracking that occurred during transport. Initially, the model was calibrated solely based on the fundamental periods experimentally identified before the shaking table tests. Table 8 shows the fundamental frequencies and corresponding modal masses for both models. These values are then compared in Table 9 with the experimental data identified before the shaking table tests. Overall, the results show good agreement between numerical and experimental data for both models, with frequency error percentage lower than 3.5% for *Model A* and 22% for *Model B*. Since the same calibration approach was applied to both models, the reliability of the results should be assessed globally across the two. Therefore, the comparison can be considered satisfactory.

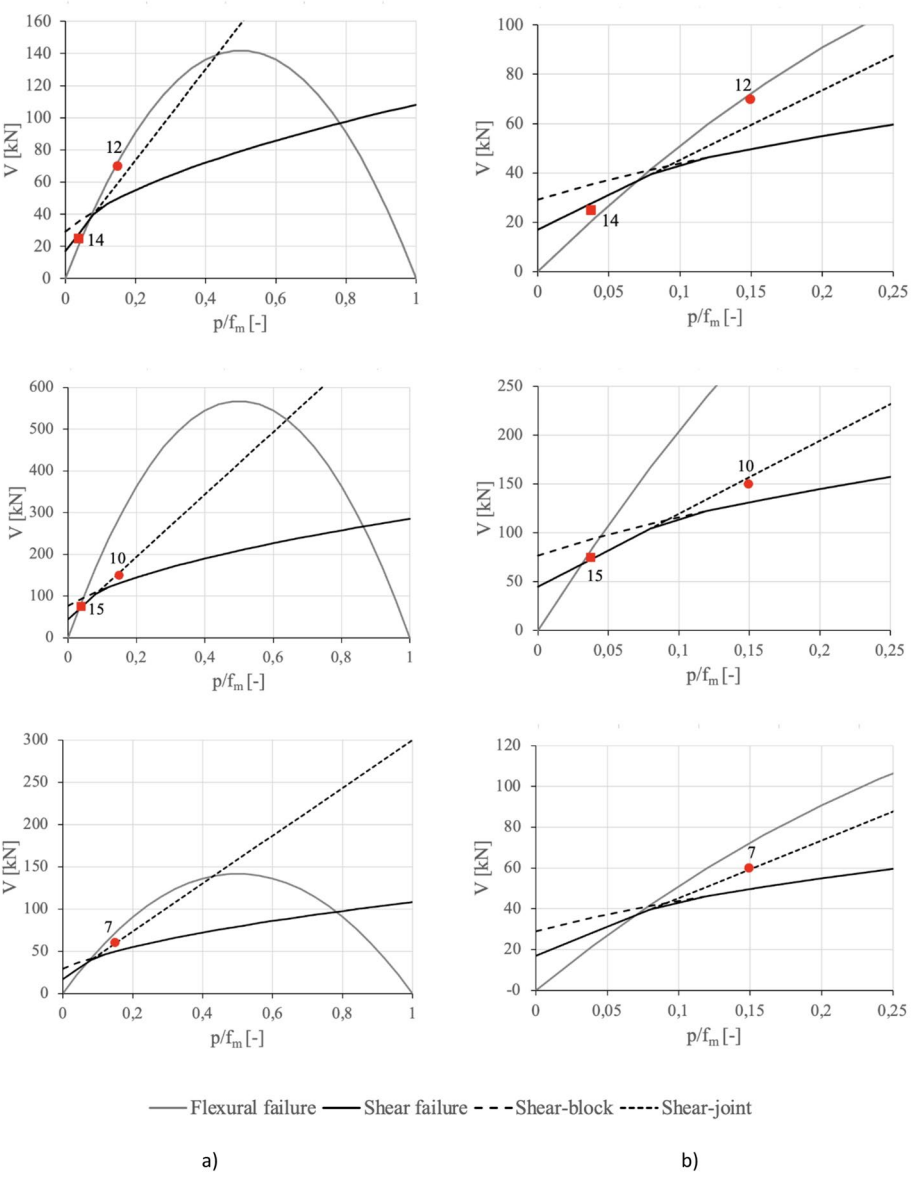

Fig. 7 Comparison between the experimental results on ESECMaSE panels and the prediction of the strength criteria adopted in the EF models: **a**) whole domain; **b**) initial part of the domain

Table 6 Comparison between experimental strength parameters (from ESECMaSE panels) and numerical ones

Parameter	$\mathbf{f_m}$[MPa]	Δ_x[m]	Δ_y[m]	μ [−]	**c**[MPa]	$\bar{\mu}$ [−]	$\bar{c}$ [MPa]	$\mathbf{f_{bt}}$[MPa]
ESECMaSE	6.7	0.365	0.250	0.600	0.240	0.329	0.132	0.380
Tremuri	5.6	0.400	0.250	0.790	0.180	0.400	0.090	0.360

Table 7 Parameters used in the nonlinear field of the numerical model

Parameter		$\theta_{E,3}$	$\theta_{E,4}$	$\theta_{E,5}$	$\beta_{E,3}$	$\beta_{E,4}$
Piers	Shear	0.003	0.005	0.007	0.7	0.4
	Flexural	0.005	0.01	0.015	0	0.85
Spandrels	Shear/Flexural	0.003	0.006	0.02	0.6	0.6

Table 8 Fundamental periods and modal masses from modal analyses in Tremuri for the two models

	Transversal mode			Longitudinal mode		
	Freq. [Hz]	Mx [kg]	My [kg]	Freq. [Hz]	Mx [kg]	My [kg]
Model A	6.89	26,636	0	5.5	0	21,403
Model B	7.04	25,665	25	5.42	50	22,013

Table 9 Comparison between experimental and numerical natural frequencies for the two models

First mode	Model A			Model B		
	Numerical freq. [Hz]	Experimental freq. [Hz]	Err [%]	Numerical freq. [Hz]	Experimental freq. [Hz]	Err [%]
Transversal	6.89	6.9	0.1	7.04	5.8	21.4
Longitudinal	5.5	5.7	3.5	5.42	5.4	0.3

4 Comparison between experimental and numerical results

This section compares experimental data with numerical results. The results are organized as follows: Sect. 4.1 compares the hysteretic cycles, damage patterns, and global failure modes. Section 4.2 presents the results obtained by applying the techniques introduced in § 2.3 to compute the natural frequencies of vibration and the evolution of top displacements. It should be noted that, to limit the computational effort of the numerical NLDAs, the time histories applied to the models were split into two sequences—transversal and longitudinal—by removing the first stage. Thus, the two sequences are defined as follows: runs 02, 03T, 04, 05T, 06, 07T, and 08 for the transversal direction; runs 02, 03L, 04, 05L, 06, 07L, and 08 for the longitudinal direction. In the NLDA, a Rayleigh damping was used by assuming a 3% of viscous damping in correspondence with the first modal period and a secant period corresponding to a cumulative participation mass higher than 80% as it represents the expected evolution of the structural response in the nonlinear range.

4.1 Comparison of hysteretic curves, damage patterns, and failure modes

Figure 8 shows the experimental (in grey) and numerical (in black) hysteretic cycles for runs with increasing PGAs. The comparison is illustrated here for *Model B* (north and south façades), though similar results were obtained for *Model A* as well. The comparison of damage patterns is shown in Fig. 9b for the same façades of this model.

The numerical curves in Fig. 8 were obtained from the NLDAs performed using the Tremuri software. In contrast, the experimental curves were derived by calculating the base shear as the sum of the inertial forces transmitted to the two floors, which were obtained by multiplying the story masses by the acceleration time histories recorded during the tests. The dynamic mass associated with each floor was derived from the Tremuri numerical model. It

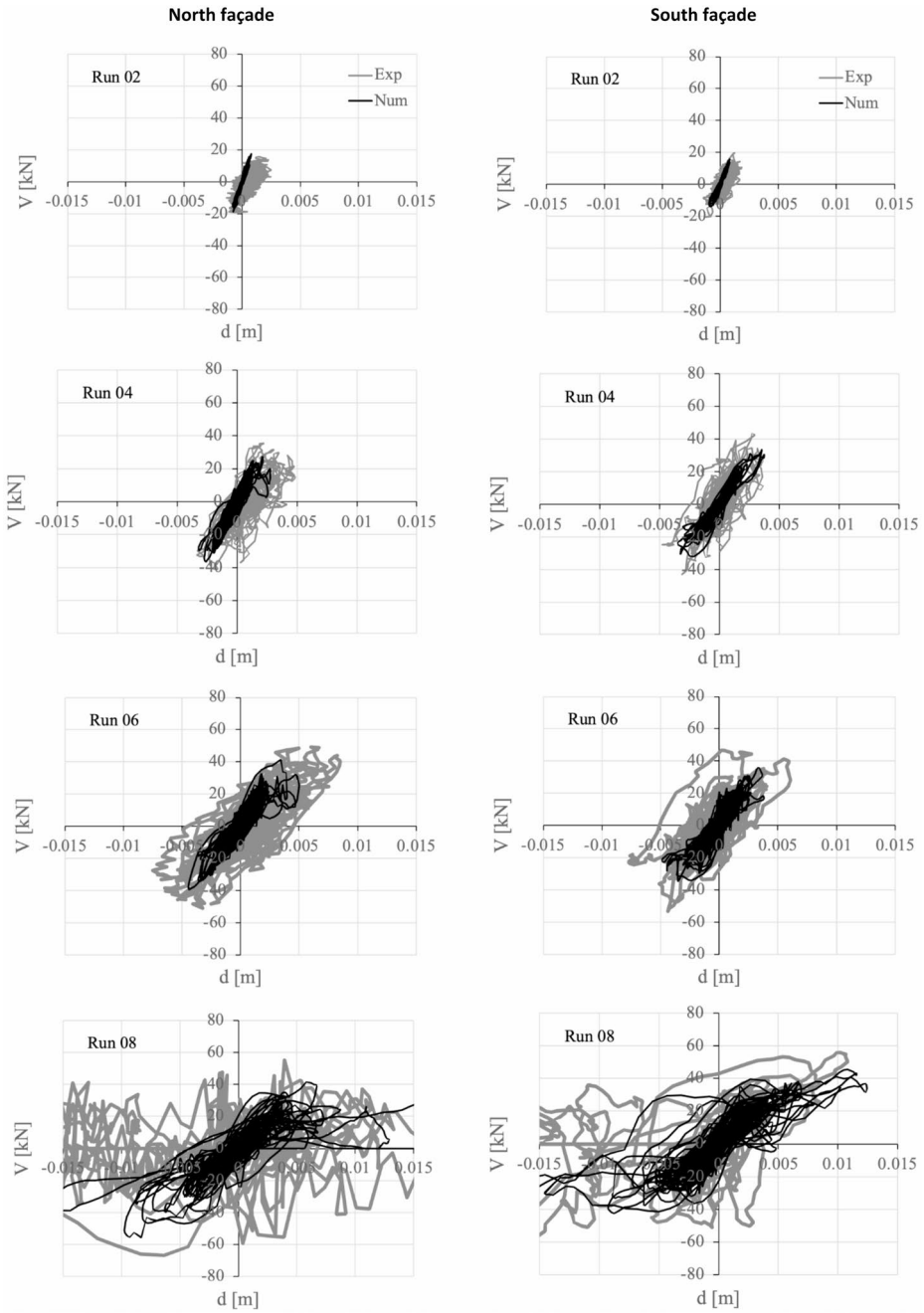

Fig. 8 Comparison of experimental (grey) and numerical (black) hysteretic curves with increasing PGA: north and south walls for *Model B*

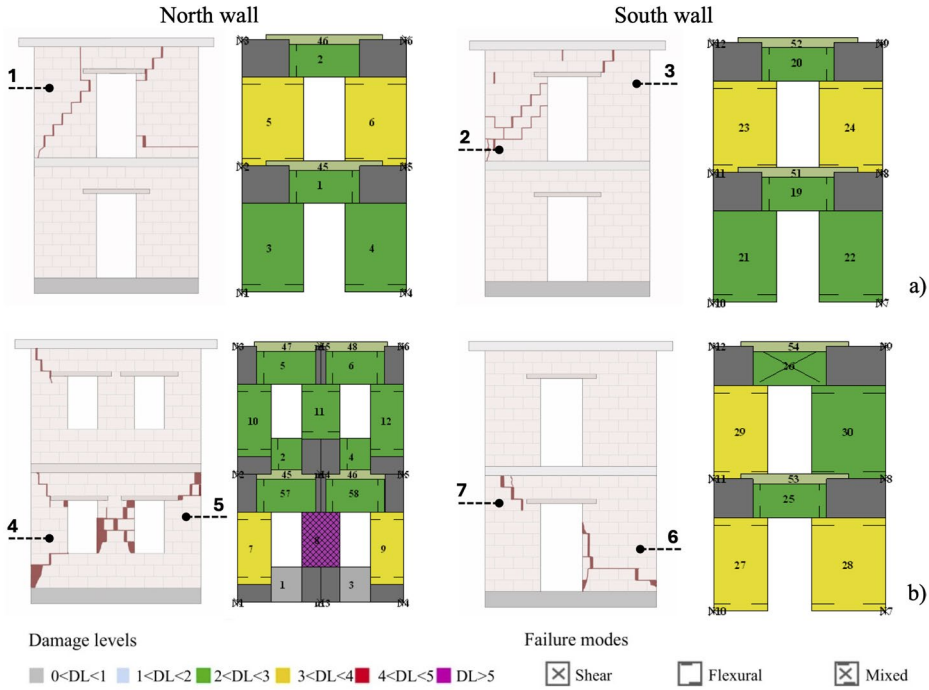

Fig. 9 Experimental and simulated damage on *Model A* (**a**) and *Model B* (**b**) for North and South façades

Fig. 10 Detected damage on *Model A* (**a**), and *Model B* (**b**) for North and South façades (IDs refer to Fig. 9). Pictures adapted from Lu et al. 2014 and Degée et al. 2014

was computed as the sum of the dynamic masses corresponding to the nodes at each level in the examined wall. It is important to note that only the dynamic mass in the relevant direction for each wall was considered—specifically, the longitudinal direction for the east and west walls, and the transversal direction for the north and south walls. Figures 8 and 9 show that experimental and numerical results align quite well overall. The hysteretic cycles illustrated in Fig. 8 show that the numerical models can consistently predict the experimental response as maximum displacement capacity and inertial forces, except for the last run 08, where the test unit almost failed (see Fig. 9); thus, the reliability of the experimental data was compromised.

Furthermore, the numerical simulations captured the global failure modes for both models. Overall, the numerical damage is consistent with the experimentally observed one, with minor discrepancies in terms of severity or localization. Specifically, for *Model A*, the EF model successfully predicts the damage in the masonry piers at the second level, as observed during the shaking table tests. However, the numerical model predicts a flexural failure mode rather than the shear failure that was experimentally observed. For *Model B*, the EF model reproduces the collapse of the central pier in the north wall at the first level. Mixed flexural and shear failures are simulated numerically in alignment with the experimental observations, even if the flexural failure is the dominant global mode, unlike in the laboratory, where failure in the piers was primarily due to the activation of a shear mechanism. Figure 9 shows the damage predicted by Tremuri on *Model A* and *Model B* compared with the experimental damage.

4.2 Comparison of natural frequencies and top displacements for increasing runs

Figure 11 compares the trend in natural frequencies with increasing measured PGA values in the transversal and longitudinal directions for runs 02, 04, 06, and 08. The experimental frequencies, obtained from the dynamic identifications carried out before each seismic test (dashed lines), are compared with those obtained by employing the MATLAB algorithm, which post-processes the numerical (in black) and experimental (in grey) data by defining an equivalent linear oscillator. It is worth noting that the experimental frequencies obtained with this technique have been verified to be consistent with those derived from a frequency domain analysis. The results shown in Fig. 11 indicate that, especially for *Model A*, the numerical models tend to underestimate the experimental frequencies in the transversal direction (see the comparison between solid lines). On the contrary, the opposite trend is observed in the longitudinal direction. Despite these discrepancies and despite the different nature of the data represented by the dashed and solid curves (which are obtained under operating conditions and during shaking of the test units, respectively), all data sets consistently identify an analogous trend in degradation and the most critical stages of the structural response, as indicated by a pronounced reduction in system stiffness.

Figure 12 compares the displacements of the second-level walls with increasing PGA values in the transversal and longitudinal directions. The values correspond to the runs 02, 04, 06, and 08. Each subplot presents the transversal (T) displacements of the South (S) and North (N) façades, as well as the longitudinal (L) displacements of East (E) and West (W) façades, for both models A and B. The experimental results are shown in black on the left side of the figure (Fig. 12a), and the numerical results are shown in grey on the right side (Fig. 12b).

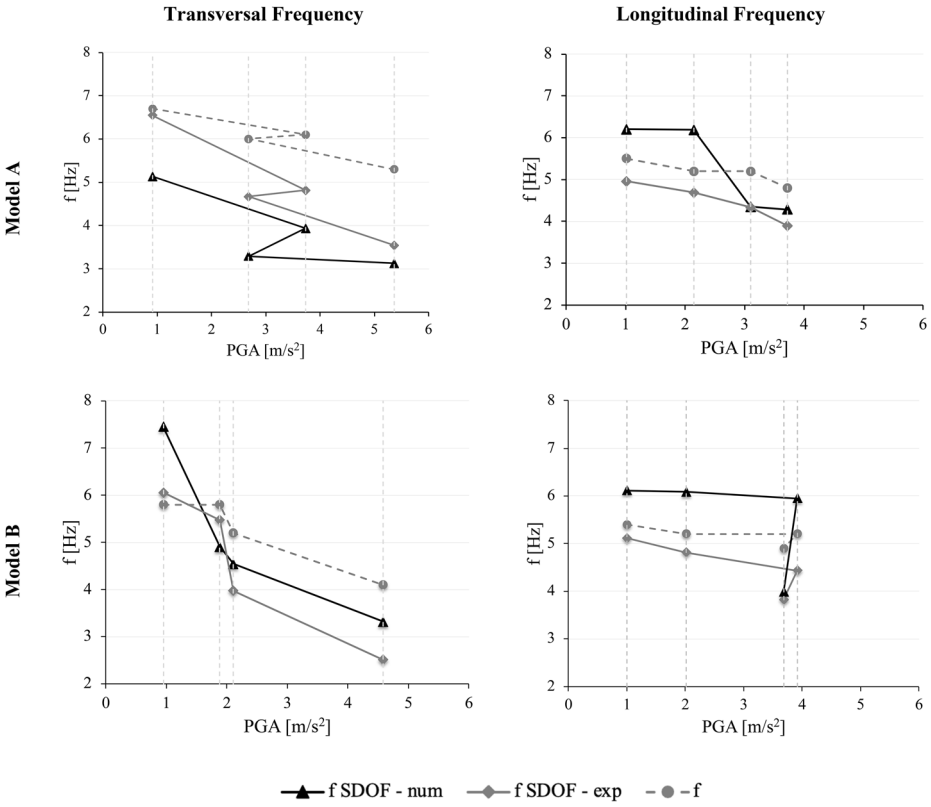

Fig. 11 Trend in frequencies with increasing PGA values (runs 02, 04, 06, 08)

Once again, the numerical model demonstrates its ability to predict the experimentally observed dynamic response. The numerical displacements generally align well with the experimental ones, showing good overall correlation. Some discrepancies appear mainly in the final runs, where the test units fail, and the data become less reliable.

To provide a global quantification of the accuracy of the numerical predictions with respect to the experimental data, the Root Mean Square Error (RMSE) was calculated according to Eq. 2, using the displacement values presented in Fig. 12:

$$RMSE = \sqrt{\frac{1}{N}\sum_{i=1}^{N}(y_i - \widehat{y_i})^2} \tag{2}$$

where N is the number of runs, and y_i and $\widehat{y_i}$ are the experimental and numerical second-level walls displacements, respectively. The RMSE values are reported in Table 10 for both models and directions, considering the transversal (T) displacements of the South (S) and

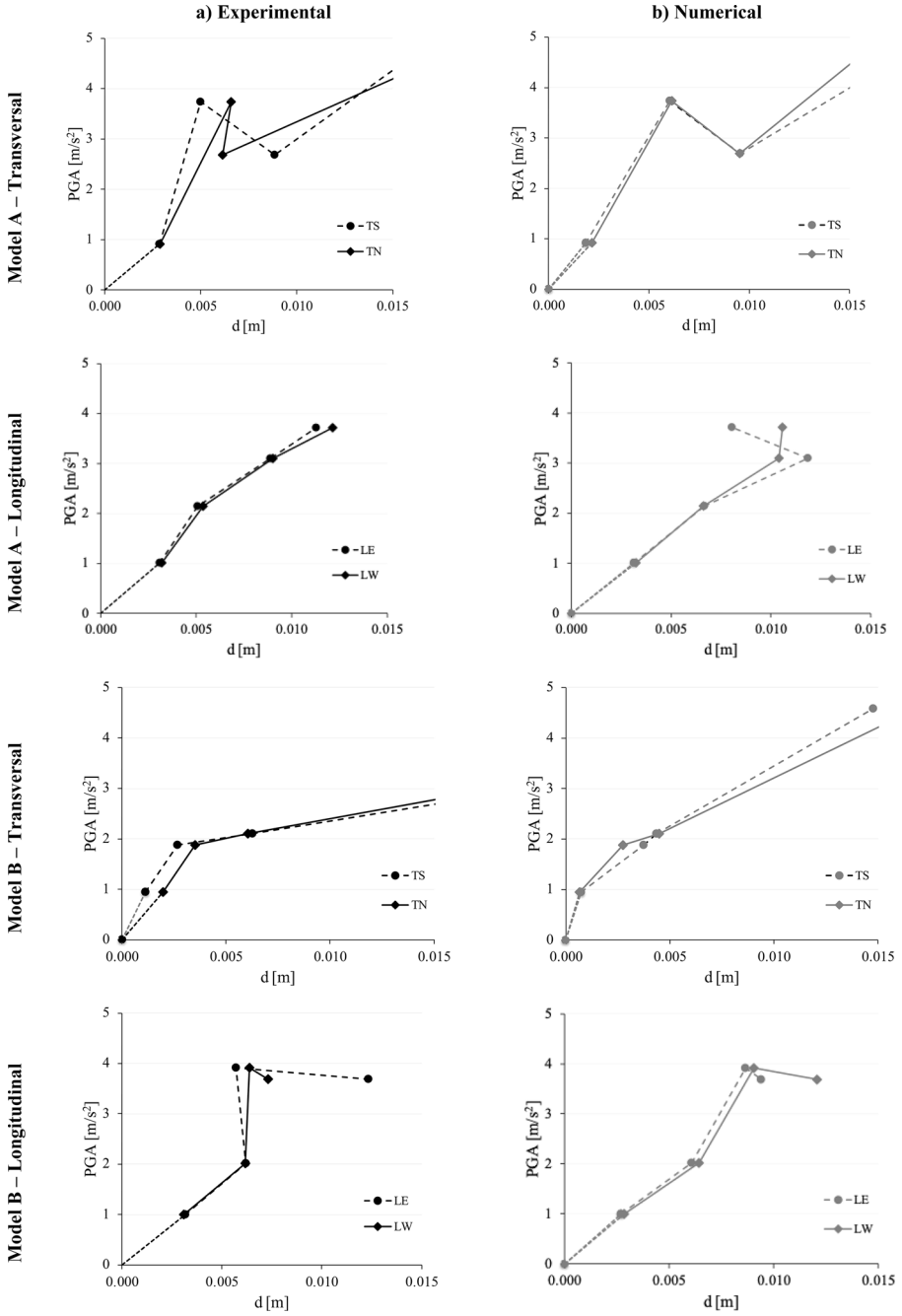

Fig. 12 Comparison between second-level walls displacements from NLDA with increasing PGA values: experimental (**a**) vs. numerical (**b**) results corresponding to runs 02, 04, 06, 08

Table 10 RMSE of second-level walls displacements compared for both models and directions (the values shown in parentheses were calculated excluding the last run)

Model A				Model B			
Transversal		Longitudinal		Transversal		Longitudinal	
TS [mm]	TN [mm]	LE [mm]	LW [mm]	TS [mm]	TN [mm]	LE [mm]	LW [mm]
1.31	2.67	2.34	1.23	14.41 (1.29)	11.19 (1.25)	2.10	2.74

North (N) façades, as well as the longitudinal (L) displacements of the East (E) and the West (W) façades.

Overall, Table 10 shows low values for the RMSE, confirming the reasonableness of numerical predictions. The accuracy is high, especially for *Model A*, and for the initial runs of the response, which were linear or moderately nonlinear. Higher RMSE values are observed only for the transversal response of *Model B*, which experienced the most severe damage. This increase is mainly attributable to the final run (run 08), where the test unit almost failed, and the acquisition of experimental results was no longer reliable. Indeed, when the RMSE is recalculated excluding the last run (values shown in parentheses in Table 10), the results are comparable to those obtained for *Model A* and for the longitudinal direction of *Model B*, confirming the robustness of the numerical model.

$$V = \sum_{k=1}^{n} \phi_k \left({\phi_k}^T V \right) = \sum_{k=1}^{n} \phi_k Y_k \tag{3}$$

Finally, to further quantify the agreement between numerical predictions and experimental data, the Proper Orthogonal Decomposition (POD) technique (Lumley 1970) was applied to the displacement time histories of *Model B*, as shown in Fig. 13. This tool provided a schematic representation of the deformed shapes of the North and East façades at different runs. The POD technique, previously used in other engineering applications (e.g., Solari et al. 2007), was first applied in the field of seismic assessment by Lagomarsino and Cattari (2015) to interpret the dynamic response of structures subjected to earthquakes in terms of dominant behaviors. As extensively described in Lagomarsino and Cattari (2015), the POD aims to represent a random process as a linear combination of deterministic quantities (modes) modulated by random uncorrelated coefficients (Principal Components - PCs). This is obtained through a non-parametric modal expansion. To apply this technique, the results from NLDA are first organized into a data matrix **V**, whose columns contain the signal time histories such that each row corresponds to the variables observed at the same time. Then, the matrix is decomposed through a basis of orthonormal vectors (φ) to obtain a new matrix with uncorrelated components:

The components Y_k of **V** on the basis φ are the PCs, while the basis used is the covariance matrix (**C**). By solving the eigenvalue problem formulated in Eq. 4, the eigenvectors φ and the eigenvalues λ of the covariance matrix **C** can be determined, and it is possible to define the response modes and the energy associated with each mode, respectively.

Fig. 13 shows the deformed shapes of the North and East façades of *Model B* at different runs.

$$(\mathbf{C} - \lambda \mathbf{I})\, \phi = 0 \tag{4}$$

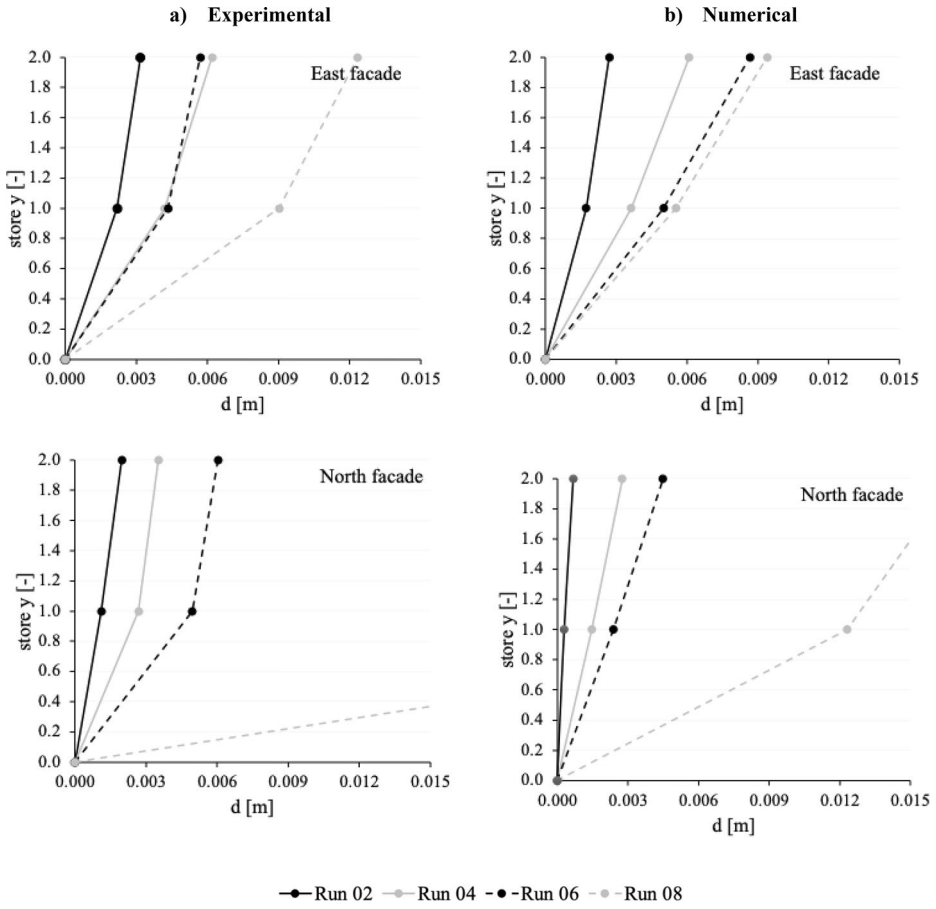

Fig. 13 Deformed shapes in elevation of the East end North façade of *Model B* obtained applying the POD technique to the experimental (**a**) and numerical (**b**) displacements for increasing runs

From the figure, it can be observed that, for the East façade, the numerical model can capture a deformed shape characterized by more pronounced displacements at the ground floor from the outset, consistent with the experimental response. For the North façade, the simulation successfully reproduces the final global failure mechanism. However, during the initial runs, a more pronounced linear response is observed compared to the experimental results.

5 Conclusions

The paper addresses the challenging task of using nonlinear numerical modeling to predict the seismic response of existing masonry structures, a topic of relevance to both researchers and practitioners, due to its potential impact on engineering practice. To this end, it presents the results of the numerical simulation of a shaking table test campaign performed on two full-scale masonry prototypes at Laboratório Nacional de Engenharia Civil (LNEC) in Lisbon. To address the challenge of setting up a reliable numerical model starting from lim-

ited data from geometry, constructive details, and material characterization, the equivalent frame (EF) modeling strategy was chosen, as it offers a satisfactory balance between computational effort and result accuracy. The numerical model was created using the approach employed in blind prediction studies, replicating a process similar to that used by practitioners in the seismic assessment of existing buildings. First, appropriate modeling strategies were implemented to describe the nonlinear behavior of the structural elements, based on widely accepted criteria and an analysis of the construction details. A piecewise-linear constitutive law based on a phenomenological approach was applied to describe the nonlinear response up to severe damage levels. Moreover, as a novel contribution of this study, the *flange effect* was modelled by introducing an equivalent beam that couples the nodes at the top of the orthogonal piers. This beam was properly calibrated using the practice-oriented formula proposed by Cattari et al. 2023 as a function of the geometry and material properties of the *web* and the *flange*. Then, to calibrate the parameters at the scale of the structural elements on which EF models are based, the data from experimental tests on panels built with a similar masonry were used. Next, the results obtained from nonlinear dynamic analyses (NLDAs), which replicated the shaking table tests, were compared with experimental data to validate the numerical model. While the validation of the EF approach in this paper is limited to modern masonry typologies with box-like behaviour—which nonetheless represent the most appropriate application domain for this modeling strategy—experimental studies on such typologies remain relatively rare. Therefore, this validation constitutes a further novel contribution and enforces the reliability of the EF modeling approach. Finally, to gain insights into the seismic behavior of the prototypes and manage the large amount of experimental data obtained, traditional and more innovative techniques were synergically applied, including frequency analysis and the identification of an equivalent linear system.

Overall, a good agreement was observed between the experimental and numerical results across the full set of data and both simulated models, without the need for further refinement or tuning. The main findings can be summarized as follows:

- The numerical model was able to predict the modal dynamic properties of the test units identified before the shaking table tests, with very low frequency error percentages, below 3.5%, except for *Model B* in one direction.
- The numerical model successfully reproduced the experimental hysteretic response, both in terms of maximum displacement capacity and inertial forces, as well as the experimentally observed global failure mechanisms. Moreover, overall, the numerically simulated damage patterns were consistent with the experimental observations, with minor discrepancies in terms of severity or localization.
- The numerical model captured the key stages of the structural response, successfully reproducing the stiffness degradation with increasing PGA values. A slight overestimation was observed in the longitudinal direction for both models, and a slight underestimation in the transversal direction, particularly for *Model A*.
- The comparison between experimental and numerical second-level wall displacements for increasing PGA values confirmed the reliability of the numerical predictions, with Root Mean Square Error (RMSE) values below 2.67 mm for *Model A* and 2.74 mm for *Model B*, when excluding the final run, during which the test unit was close to failure, and the experimental data were no longer reliable.

These findings proved that the EF strategy seems reliable and robust in describing the seismic response of both symmetric and asymmetric configurations of the two experimental prototypes, demonstrating its capability to reproduce the progression of nonlinear behavior as well.

Acknowledgements The European Union Seventh Framework Programme (FP7/2007–2013) provides funding for the shake table experimental campaign, under Grant Agreement No. 227887, SERIES. The authors thank the colleagues of LNEC (Earthquake Engineering Division) who carried out the tests, as well as Dr. Jaeger from Wienerberger and Dr. Lu, for the project coordination and for the test material supply. Finally, the authors thank A. Chioccarello for her help with the analyses, and C. Mordant, who assisted her during her stay period in Belgium and collaborated on this research.

Author contributions SDA: material preparation and data collection; writing original draft. HD: experimental tests; writing-review & editing. SL and SC: analysis; software; supervision; writing-review & editing.

Funding Open access funding provided by Università degli Studi di Genova within the CRUI-CARE Agreement. Open access funding provided by the University of Genoa. The authors declare that no other funds or support were received during the preparation of this manuscript.

Data availability The datasets generated during and/or analysed during the current study are available from the corresponding author on reasonable request.

Declarations

Competing interests The authors have no relevant financial or non-financial interests to disclose.

Open Access This article is licensed under a Creative Commons Attribution 4.0 International License, which permits use, sharing, adaptation, distribution and reproduction in any medium or format, as long as you give appropriate credit to the original author(s) and the source, provide a link to the Creative Commons licence, and indicate if changes were made. The images or other third party material in this article are included in the article's Creative Commons licence, unless indicated otherwise in a credit line to the material. If material is not included in the article's Creative Commons licence and your intended use is not permitted by statutory regulation or exceeds the permitted use, you will need to obtain permission directly from the copyright holder. To view a copy of this licence, visit http://creativecommons.org/licenses/by/4.0/.

References

Aşıkoğlu A, Vasconcelos G, Lourenço PB, Pantò B (2020) Pushover analysis of unreinforced irregular masonry buildings: lessons from different modeling approaches. Eng Struct 218:110830

Aşıkoğlu A, D'Anna J, Lourenço Ramirez R, Solarino F, Romanazzi A, Ciocchi MP, Bianchini N (2024) Simulation of blind pre-diction and post-diction shaking table tests on a masonry building aggregate using a continuum modelling approach. Bull Earthq Eng 22:6163–6193

Bartoli G, Betti M, Biagini P et al (2017) Epistemic uncertainties in structural modeling: a blind benchmark for seismic assessment of slender masonry towers. J Perform Const Facilit 31:04017067

Betti M, Galano L, Vignoli A (2015) Time-history seismic analysis of masonry buildings: a comparison between two non-linear modelling approaches. Buildings 5:597–621

Bianchini N, Ciocci MP, Solarino F, Romanazzi A, Ramirez R, D'Anna J, Aşıkoğlu A (2024) Influence of wall–to–floor connections and pounding on pre– and post–diction simulations of a masonry building aggregate tested on a shaking table. Bull Earthq Eng 22:6141–6161

Bracchi S, Rota M, Penna A, Magenes G (2015) Consideration of modelling uncertainties in the seismic assessment of masonry buildings by equivalent-frame approach. Bull Earthq Eng 13:3423–3448

Brunelli A, de Silva F, Piro A, Parisi F, Sica S, Silvestri F, Cattari S (2020) Numerical simulation of the seismic response and soil-structure interaction for a monitored masonry school building damaged by the 2016 Central Italy earthquake. Bull Earthq Eng 1–31

Calderini C, Cattari S, Lagomarsino S (2009) In-plane strength of unreinforced masonry piers. Earthq Eng Struct Dynam 38:243–267

Calderini C, Bianchini N, Lourenço PB et al (2024) Shake-Table Testing of a Brick Masonry Groin Vault: Overview of Blind Predictions and Postdictions and Comparison with Experimental Results. Int J Architectural Herit 18:12

Cattari S, Lagomarsino S (2013) Masonry structures in developments in the field of displacement based seismic assessment, Edited by Sullivan TJ, Calvi GM, IUSS Press, Pavia, Italy, 151–200 and 464 EUCENTRE, p. 524, ISBN; 978-88-6198-090-7

Cattari S, Magenes G (2022) Benchmarking the software packages to model and assess the seismic response of unreinforced masonry existing buildings through nonlinear static analyses. Bull Earthq Eng 20:1901–1936

Cattari S, Chioccariello A, Degée H, Doneux C, Lagomarsino S, Mordant C (2014) Seismic assessment of masonry buildings from shaking table tests and nonlinear dynamic simulations by the proper orthogonal decomposition (POD), Proceedings of the 2ECEES conference, 24–29 August, Istanbul

Cattari S, Camilletti D, D'Altri AM, Lagomarsino S (2021) On the use of continuum Finite Element and Equivalent Frame models for the seismic assessment of masonry walls. J Building Eng 43:102519

Cattari S, Calderoni B, Caliò I, Camata G, de Miranda S, Magenes G, Milani G, Saetta A (2022) Nonlinear modelling of the seismic response of masonry structures: critical review and open issues towards engineering practice. Bull Earthq Eng 20:1939–1997

Cattari S, Alfano S, Lagomarsino S (2023) A practice-oriented proposal to consider the flange effect in equivalent frame modeling of masonry buildings. Buildings 13:462

D'Altri AM, Sarhosis V, Milani G, Rots J, Cattari S, Lagomarsino S, Sacco E, Tralli A, Castellazzi G, de Miranda S (2020) Modeling strategies for the computational analysis of unreinforced masonry structures: review and classification. Arch Comput Methods Eng 27(4):1153–1185

D'Altri AM, Cannizzaro F, Petracca M, Talledo DA (2021) Nonlinear modelling of the seismic response of masonry structures: Calibration strategies. Bull Earthq Eng. https://doi.org/10.1007/s10518-021-01104-1

Degée H, Deno ël V, Candeias P, Costa AC, Coelho E (2007) Experimental investigation on the seismic behaviour of north European masonry houses, Proceedings of SÍSMICA 2007–7º Congresso De Sismologia e Engenharia Sísmica

Degée H, Mordant C, Candeias P, Mendes L, Costa AC, Coelho E, Suikai L, Jaeger A (2014) Seismic performances of modern unreinforced thermal insulation clay blocks masonry houses, Proceedings of EURODYN 2014. 30 June – 2 July, Porto

Degli Abbati S, Morandi P, Cattari S, Spacone E (2022) On the reliability of the equivalent frame models: the case study of the permanently monitored Pizzoli's town hall. Bull Earthq Eng 1–31. https://doi.org/10.1007/s10518-021-01145-6

EN 1998-3 (2005) Eurocode 8: Design of structures for earthquake resistance - Part 3: Assessment and retrofitting of buildings, CEN (European Committee for Standardization), Brussels, Belgium

Esposito R, Messali F, Ravenshorst GJ et al (2019) Seismic assessment of a lab-tested two-storey unreinforced masonry Dutch terraced house. Bull Earthq Eng 17:4601–4623

Ferrero C, Degli Abbati S, Cattari S, Lagomarsino S (2024) A novel strategy for the equivalent frame modelling of masonry arches in historic buildings: application to a case study. Int J Architectural Herit. https://doi.org/10.1080/15583058.2024.2385970

Giamundo V, Sarhosis V, Lignola G et al (2014) Evaluation of different computational modelling strategies for the analysis of low strength masonry structures. Eng Struct 73:160–169

Jäger A, Lu S, Degée H, Mordant C, Chioccariello A, Rakicevic ZT, Sendova V, Mendes L, Candeias P, Campos Costa A, Correia AA, Coelho E, Geotechnical (2015) Geol Earthq Engineering), volume 35

Lagomarsino S, Cattari S (2015) Seismic performance of historical masonry structures through pushover and nonlinear dynamic analyses. Geotechnical, Geological and Earthquake Engineering 39, 2ECEES book (Ed. A. Ansal). Springer

Lagomarsino S, Penna A, Galasco A, Cattari S (2013) TREMURI program: an equivalent frame model for the nonlinear seismic analysis of masonry buildings. Eng Struct 56:1787–1799

Lourenco PB (2002) Computations on historic masonry structures: Historic Masonry Structures. Prog Struct Eng Mater 4:301–319

Lu S, Jaeger A, Degèe H, Mordant C, Chioccariello A, Rakizevic Z, Sendova V, Candeias P, Mendes L, Campos Costa P, Coelho E (2014) Full-scale shaking table tests of two-storey modern thermal insulation clay block masonry buildings including nonlinear pushover analysis, Proceedings of the 2ECEES conference, 24–29 August, Istanbul

Lumley JL (1970) Stochastic tools in turbulence. Academic, New York

Malcata M, Ponte M, Tiberti S et al (2020) Failure analysis of a Portuguese cultural heritage masterpiece: Bonet building in Sintra. Eng Fail Analy 115:104636

Malomo D, DeJong MJ (2022) M-DEM simulation of seismic pounding between adjacent masonry structures. Bull Earthq Eng. https://doi.org/10.1007/s10518-022-01545-2
Mann A, Müller H (1982) Failure of shear-stressed masonry- an enlarged theory, tests and application to shear walls. Proc Br Ceram Soc 30:223–235
Marino S, Cattari S, Lagomarsino S, Dizhur D, Ingham J (2019) Post-earthquake damage simulation of two colonial unreinforced clay brick masonry buildings using the equivalent frame approach. Structures 212–226
Marques R, Lourenço PB (2011) Possibilities and comparison of structural component models for the seismic assessment of modern unreinforced masonry buildings. Comput Struct 89:2079–2091
Mendes L, Candeias P, Correia A, Costa AC, Coelho E, Jäger A, Lu S, Degée H, Mordant C (2014) Full-scale seismic testing of modern unreinforced thermal insulation clay block masonry houses, Proc. of the 9th Int. Masonry Conf, Guimarães
Mendes N, Costa AA, Lourenço PB et al (2017) Methods and approaches for blind test predictions of out-of-plane behavior of masonry walls: a numerical comparative study. Int J Architect Herit 11:1
Morandi P, Albanesi L, Graziotti F, Piani TL, Penna A, Magenes G (2018) Development of a dataset on the in-plane experimental response of URM piers with bricks and blocks. Constr Build Mater 190:593–611
NTC (2018) Italian Technical Code, D.M. 17/1/2018. Aggiornamento delle << Norme tecnicheper le costruzioni >>., Ministry of Infrastructures and Transportation, G.U. n.42 of 20/2/2018 (In Italian)
Ottonelli D, Manzini CF, Marano C, Cordasco EA, Cattari S (2022) A comparative study on a complex URM building: part I—sensitivity of the seismic response to different modelling options in the equivalent frame models. Bull Earthq Eng 20:2115–2158
Parisse F, Cattari S, Marques R et al (2021) Benchmarking the seismic assessment of unreinforced masonry buildings from a blind prediction test. Structures 31:982–1005
Parisse F, Marques R, Cattari S, Lourenço PB (2022) Finite Element and Equivalent Frame modeling approaches for URM buildings: Implications of different assumptions in the seismic assessment. J Building Eng 61:105230
Requena-Garcia-Cruz MV, Cattari S, Bento R, Morales-Esteban A (2023) Comparative study of alternative equivalent frame approaches for the seismic assessment of masonry buildings in OpenSees. J Building Eng 66:105877
Roca P, Cervera M, Gariup G, Pelà L (2010) Structural analysis of masonry historical constructions. Classical and advanced approaches. Arch Comput Methods Eng 17(3):299–325
Rota M, Penna A, Magenes G (2014) A framework for the seismic assessment of existing masonry buildings accounting for different sources of uncertainty. Earthq Eng Struct Dyn 43:7
Solari G, Carassale L, Tubino F (2007) Proper Orthogonal Decomposition in wind engineering: Part 1: A state-of-the-art and some prospects. Wind Struct 10(2):153–176
Tomic I, Candeias PX, Penna A et al (2024) Shake-table testing of a stone masonry building aggregate: overview of blind prediction study. Bull Earthq Eng 22:5993–6035
Tomić I, Beyer K (2024) Shake-table test on a historical masonry aggregate: prediction and postdiction using an equivalent-frame model. Bull Earthq Eng 22:6225–6258
Van Overschee P, De Moor B (1994) N4SID: Subspace algorithms for the identification of combined deterministic-stochastic systems. Automatica Special Issue Stat Process Control 30:1

Publisher's note Springer Nature remains neutral with regard to jurisdictional claims in published maps and institutional affiliations.

Authors and Affiliations

Stefania Degli Abbati[1] · Hervé Degée[2] · Sergio Lagomarsino[1] · Serena Cattari[1]

✉ Stefania Degli Abbati
stefania.degliabbati@unige.it

Hervé Degée
herve.degee@uhasselt.be

Sergio Lagomarsino
sergio.lagomarsino@unige.it

Serena Cattari
serena.cattari@unige.it

[1] DICCA, Department of Civil, Chemical Environmental Engineering, University of Genova, Via Montallegro 1, 16145 Genova, Italy

[2] Construction Engineering Research Group, Hasselt University, Geb. H, Diepenbeek 3590, Belgium